# Mechanical displacement induced in a piezoelectric structure: Experimental measurement by laser interferometry and simulation by a finite element method

Marcel Gindre,[a] Wladimir Urbach,[a] Roger H. Coursant, and Mathias Fink[b]
*Laboratoires d'Electronique et de Physique appliquée,[c] 94450 Limeil-Breviannes, France*

From the knowledge of piezoelectric material tensorial components one can, by the finite element method, calculate the electrical impedance versus frequency and simulate the mechanical deformation of piezoelectric bars. Here, the simulation results obtained with lead zirconate-titanate and lead titanate ceramics are reported. In order to check the validity of the simulation, interferometric measurements of the mechanical deformation amplitude were performed. It is shown that these measurements are able to reveal the inhomogeneity of the materials under study and that a small error in the tensorial parameter absolute values leads to an inconsistent picture of simulated mechanical deformation.

PACS numbers: 43.88.Ar, 43.88.Fx, 43.85.Vb, 43.35.Yb

## INTRODUCTION

During the past years, the quality of ultrasonic imaging in medicine has been considerably improved thanks to signal processing and electronic skill. Further improvements will probably be due to transducer optimization.[1] Computer calculations allow the optimization of piezoelectric structures with respect to their electromechanical conversion qualities and to their vibration modes. These simulations exploit either one-dimensional or two-dimensional models.[2,3] Two-dimensional modeling is necessary to optimize the design of up-to-date, real time, electronically scanned transducers like the ones used in ultrasonic medical imaging. One of the drawbacks to these approaches based on simulation is the use of simplifying asumptions implicitly made by fitting the characteristics of the simulated state of vibration to the ones of an equivalent one-dimensional thickness-mode state of vibration (i.e., the so-called Mason's mode). It is then important to compare the calculated results with the direct measurements of the vibrating transducer deformation.

To our knowledge, although there have been some attempts to correlate the predicted modes of piezoelectric structure vibrations with experimental measurements, most studies concern disk shaped transducers that allow analytical calculation. For parallelepipedic transducers, most authors have been interested only in comparison of calculated and measured resonance frequencies and not in the transducer mechanical deformation that contains valuable information for transducer design.[4] One of the more complete works done in this field is by Jungerman *et al.*[5] The authors, however, were rather interested in the general shape of the deformation calculated by the variational method. They do not provide the absolute values of either the estimated displacement amplitudes or the measured ones. Furthermore, in some cases a polymer film was stacked at the front of the transducer in order to increase the reflectivity for interferometric measurements; hence, the authors might bias the measured values of the transducer front plane displacements.

We have simulated the vibrations of two parallelepipedic transducers with identical geometrical shapes but made from two different piezoelectric materials. Both are commercially available under the following designations: PXE-5 (Philips), a commonly used lead zirconate-titanate piezoceramic, and C-24 (Toshiba), a lead titanate piezoceramic with a modified composition leading to a strong electromechanical anistropy that enhances pure compressional thickness mode.[4] The simulation has been performed using a finite element method software package extended to the calculation of the state of vibration of piezoelectric structures.[6] The calculated results have been compared with the direct measurements of the mechanical displacement amplitude by means of a laser interferometer.[7]

After a brief description of the interferometer setup, we shall describe shortly the principle of the simulation. The results obtained by interferometry and simulation will be presented in Sec. III and discussed in Sec. IV.

## I. OPTICAL SETUP DESCRIPTION

The description of the heterodyne interferometer operation is aided by reference to Fig. 1. A coherent beam from an He–Ne laser passes through an acoustic cell driven at a frequency $f_R = \omega_R/2\pi = 70$ MHz, which is much higher than any expected motion frequency of the transducer under study. The acoustic cell acts as a phase grating and gives rise to diffracted beams. The direct beam frequency is unshifted while the frequency of the first-order diffracted beam is shifted by an amount $f_R$. Hereafter, the intensities of the reference and target beams will be called $I_R$ and $I_T$, respectively.
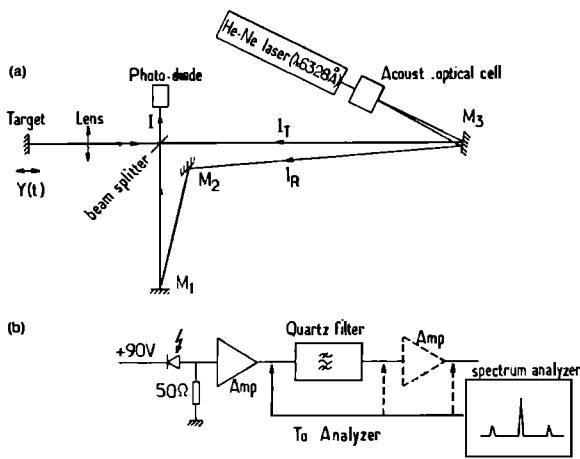
FIG. 1. (a) Schematic representation of the heterodyne interferometer; $M_1$, $M_2$, and $M_3$ are the mirrors. (b) Schematic representation of the signal detection. Depending on the detection mode, three different signal processings are indicated.

After the reflection upon a face of the transducer, the target beam is combined with the reference beam on the photodiode. The photodiode output current $I(t)$ is proportional to the light intensity

$$I(t) = |E_R(t) + E_T(t)|^2,$$

where the electric fields are $E_R = E_{R0} \cos[(\omega - \omega_R)t]$ and $E_T = E_{T0} \cos(\omega t + \phi)$.

Setting $|E_K|^2 = I_K$ ($K = R$ or $T$), one gets

$$I = I_R + I_T + 2m(I_R I_T)^{1/2}\cos[\omega_R t + \phi(t)], \quad (1)$$

where $\phi(t)$ carries the information of the transducer vibration and $m$ takes into account the interferometer imperfections such as wave front mismatch, losses in coherence, etc.

If the target displacement from its average position is described by $y(t)$, then $\phi(t) = \phi_0 + 2ky(t)$, where $\phi_0$ is the phase difference measured when $y(t) = 0$ and $k = 2\pi/\lambda$ ($\lambda = 632.8$ nm). With

$$\phi(t) = \phi_0 + 2kY\sin(\omega_T t), \quad (2)$$

the last term in Eq. (1) becomes

$$I_3 = 2m(I_R I_T)^{1/2} \cos[\omega_R t + \phi_0 + 2kY\sin(\omega_T t)]. \quad (3)$$

For $kY \ll 1$, we obtain

$$\begin{aligned} I_3 = 2m(I_R I_T)^{1/2}&\{\cos(\omega_R t + \phi_0) + kY \\ &\times\{\cos[(\omega_R + \omega_T)t + \phi_0] \\ &- \cos[(\omega_R - \omega_T)t + \phi_0]\}\}. \end{aligned} \quad (4)$$

Equation (4) shows that, in in the frequency domain, the photodiode output will display three peaks: the carrier at $\omega_R$ and two sidebands separated from the carrier by $\pm\ \omega_T$ (Fig. 1).

The photodiode was purchased from EG&G (1-ns rise time). The signal passes through a controlled voltage amplifier system (low noise and bandwidth ~400 MHz) and the output is fixed at a preset level (10 dB re: 1 mW) and sent to

a spectrum analyzer. As derived from Eq. (4), the ratio of the sideband amplitude to the carrier amplitude directly gives the target's vibrational amplitude $Y$. Because the dynamic range of the analyzer is limited to 70 dB, an alternative system has to be used when small $Y$ values ($10^{-2}$ nm) must be measured: The signal is then filtered and only one of the sidebands is sent to the spectrum analyzer. Without further amplification or averaging, the lowest measured value was $Y = 10^{-3}$ nm (Fig. 2).

## II. PRINCIPLE OF NUMERICAL SIMULATION

The use of a finite element method in structural analysis started in the 1950s but its application to simulate the state of piezoelectric structure vibrations is more recent. Roughly, the finite element method[8] is a method of transformation and approximation of a problem presented in an integral formulation, by the problem of linear algebraic formulation, where the coefficients are integral evaluations of the subareas (finite elements) of the area of resolution. Generally, the problem to be solved is expressed in a differential formulation and the integral formulation is obtained by means of the values of generalized functions defined on an appropriate
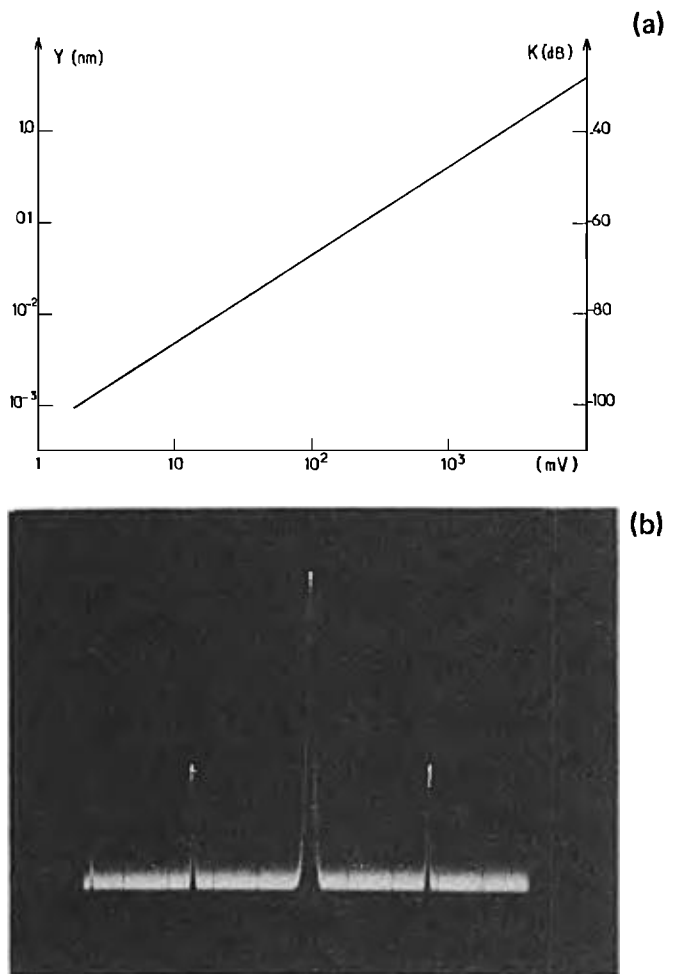


FIG. 2. (a) Mechanical displacement amplitude versus transducer applied voltage: $V_0 \sin 2\pi f t$ ($f = 2.3$ MHz) and (b) typical spectrum corresponding to $Y = 1$ nm.

vector space of test functions or, in a smaller manner, by means of a variational formulation. The convergence of the method is achieved for elliptic problems[9] and for some classes of parabolic problems.[10] In other cases, the convergence must be studied case by case. Consequently, it is not always possible to limit the error of approximation. The coefficient matrix of associated linear algebraic problems is generally a band or triangular matrix of large dimensions. This permits the use of iterative resolution of methods such as the methods of Gauss, Gauss–Seidel, or Cholesky. Figure 3 shows in schematic manner the approach used in the application of the finite element method.

When applied to the constitutive equations of piezoelectricity, the finite element methods lead to the so-called $K$-type finite element matrix formulation[6]

$$\begin{pmatrix} M_{uu} & 0 \\ 0 & 0 \end{pmatrix}\begin{pmatrix} U \\ \phi \end{pmatrix} + \begin{pmatrix} K_{uu} & K_{u\phi} \\ K_{u\phi}^T & -K_{\phi\phi} \end{pmatrix}\begin{pmatrix} U \\ \phi \end{pmatrix} = \begin{pmatrix} F \\ Q \end{pmatrix}. \quad (5)$$

The $Q$ and $F$ column vector components are the electric charges and mechanical forces, respectively, on surface nodes, whereas $U$ and $\phi$ are the nodel mechanical displacements and electric potentials. Here, $K_{uu}$, $K_{u\phi}$, $K_{\phi\phi}$, and $M_{uu}$ are matrices called elastic, piezoelectric, dielectric stiffness, and mass matrices, respectively. In the case of the simple piezoelectric structure considered here (cf. Fig. 4), the above equation is simplified to the so-called $H$-type formulation

$$\begin{pmatrix} H_{uu} & H_{u\phi} \\ H_{u\phi}^t & -H_{\phi\phi} \end{pmatrix}\begin{pmatrix} U \\ \phi \end{pmatrix} + \begin{pmatrix} M_{uu} & 0 \\ 0 & 0 \end{pmatrix}\begin{pmatrix} \ddot{U} \\ \ddot{\phi} \end{pmatrix} = \begin{pmatrix} F \\ q \end{pmatrix}, \quad (6)$$

where $H_{ij}$ are the generalized stiffness matrices, $U$ is the vector of nodal mechanical displacements, $\phi$ is now the electrical potential vector at the nodes of one of the electrodes
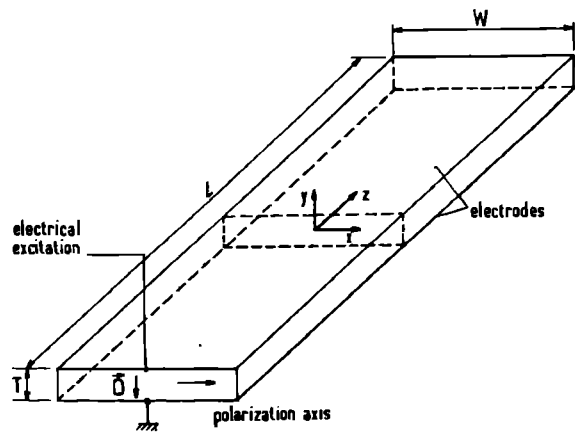


FIG. 4. Schematic representation of the transducers studied in this article. See text for more details.

(the other one is grounded), and $q$ is the electrical charge of the nongrounded electrode.

The internal attenuation in the piezoelectric material is assumed to be isotropic and frequency independent, and we consider that the structural friction force is proportional to and in quadrature with the elastic force. Thus we may define a coefficient $g$ such that the matrix expression of the structural friction force is given by

$$\widehat{R}(U) = -igH_{uu}\widehat{U}, \quad (7)$$

where the terms superimposed with the $\widehat{\phantom{x}}$ symbol are complex amplitudes of harmonic expressions [i.e., such as $U(x,t) = \widehat{U}(X,\omega)\exp(i\omega t)$].

The matrix model with structural damping is then written by

$$\begin{pmatrix} (1 + ig)H_{uu} - \omega^2 M_{uu} & H_{u\phi} \\ H_{u\phi}^t & -H_{\phi\phi} \end{pmatrix}\begin{pmatrix} \widehat{U} \\ \widehat{\phi} \end{pmatrix} = \begin{pmatrix} \widehat{F} \\ \widehat{q} \end{pmatrix}. \quad (8)$$

Note that $g^{-1}$ represents the mechanical factor $Q_m$ of the piezoelectric material (see the Appendix). By means of modal analysis, the mechanical displacement response of the system to a harmonic electrical potential excitation is given by the expansion on the pure modes

$$U(x,t) = \exp(i\omega t) \sum_{i=1}^{N} \frac{X_i^t H_{u\phi}\widehat{\phi}}{1 - \omega^2/\omega_i^2 + ig} X_i, \quad (9)$$

where $\omega_i^2$ and $X_i$, respectively, are the eigenvalues and the eigenvectors (i.e., pure modes) of the $H$-type model without radiation ($F = 0$), without internal damping ($g = 0$), and with $\widehat{\phi} = 0$ (i.e., short-circuit condition), corresponding to the harmonic equation

$$(H_{uu} - \omega^2 M_{uu})\widehat{U} = 0. \quad (10)$$

Theoretically, $N$ is infinite; in practice, $N = 15$ is generally sufficient to obtain a good estimate of $U(x,t)$.

In order to obtain a good separation between the resonances due to the length ($L$), width ($W$), and thickness ($T$) modes, we choose particular sizes for the parallelepipedic piezoelectric bars studied here: $W/T \sim 6$ and $L/W \sim 10$. Due to this particular geometry, and because we are mainly inter-
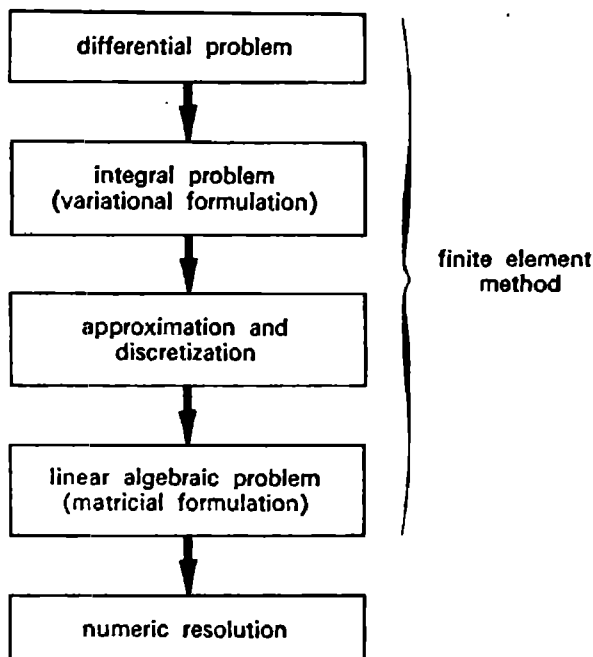


FIG. 3. Schematic representation of the finite element method.

TABLE I. Values of tensorial characteristics of the samples used in this work. For C-24, the values were obtained from Toshiba whereas, for PXE-5, the measurements were made in our laboratory. The relationship between these characteristics and the components of the $H$ matrix are given in Ref. 6.

|  | PXE-5 | C-24 |
|---|---|---|
| $g$: mechanical loss | $10^{-2}$ | $10^{-3}$ |
| $\rho$: mass density ($10^3$ kg m$^{-3}$) | 7.75 | 6.94 |
| $C^E$: elastic constants ($10^{10}$ N m$^{-2}$) | | |
| $\quad C_{11}^E$ | 13.87 | 15.0 |
| $\quad C_{13}^E$ | 8.9 | 3.2 |
| $\quad C_{33}^E$ | 12.59 | 12.7 |
| $\quad C_{44}^E$ | 3.78 | 5.5 |
| $e$: piezoelectric constants (C m$^{-2}$) | | |
| $\quad e_{13}$ | 12.87 | 3.89 |
| $\quad e_{31}$ | −5.99 | 1.61 |
| $\quad e_{33}$ | 17.7 | 8.5 |
| $\epsilon$: dielectric constants ($10^{-9}$ F m$^{-1}$) | | |
| $\quad \epsilon_{11}^S$ | 12.07 | 1.82 |
| $\quad \epsilon_{33}^S$ | 8.46 | 1.88 |

ested in the study of the thickness modes of vibration, we used a two-dimensional version of PERMAS finite element method code.[6] This version gives the mechanical displacement in the $WT$ plane and, consequently, the length modes are not taken into account. For this calculation, we exploited the knowledge of the tensorial characteristics of the samples as well as the volumic mass density ($\rho$) and the mechanical loss $Q_m = g^{-1}$. These parameters, determined experimentally for PXE-5 and obtained from Toshiba for C-24, are summarized in Table I. No mechanical loads were considered (i.e., free mechanical displacement at the boundary) and symmetry assumptions relative to the median planes can be made. As a consequence, only the positive quadrant ($X > 0$ and $Y > 0$) is used in the calculation and in the graphic representation, and the asymmetric modes of vibration are not taken into account. Thus the size element, $T \sim 0.8$ mm and $W/T \sim 6$, is divided in 65 nodes: 13 in the $W$ (or $X$)
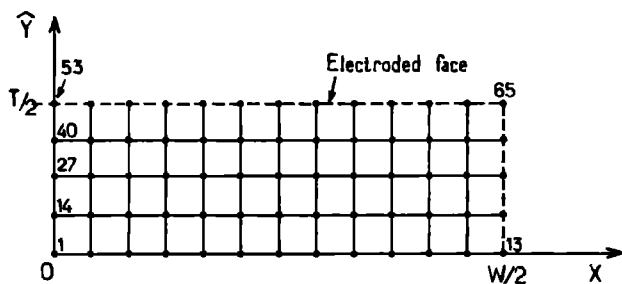


FIG. 5. Each transducer was divided into small cubic elements and the displacement value was calculated for each node. Due to the symmetry considerations, only one-fourth of the 2-D structure ($Y$ and $X > 0$) was taken into account. Node 53 corresponds to the central point of the electrode transducer face, i.e., $X = Z = 0$ and $Y = T/2$.

direction and 5 in the $T$ (or $Y$) direction (Fig. 5). As demonstrated in Ref. 6, modal analysis allows us to calculate the electrical impedance versus frequency of the piezoelectric bars considered here.

## III. RESULTS
### A. Impedance measurements and simulation

The sizes (in mm) of the elements under study obtained after sawing from larger plates and after polishing are $T = 0.822(0.830)$, $W = 4.845(4.850)$, and $L = 52.9(53)$ for PXE-5 (C24).

The measurements of the electrical impedance modulus versus frequency were carried out by means of an H. P. 3577A network analyzer. The results of the measurements are represented in Fig. 6(a) and (b); the fundamental thickness-mode frequency is 2.493 MHz for PXE-5 and 2.770 MHz for C-24.

The corresponding simulated curves, represented in Fig. 7(a) and (b), were obtained with a value of $T = 0.8$ mm for both materials. The resonance frequency obtained by simulation is 2.522 MHz for PXE-5. For C-24, a multimodality is observed in the neighborhood of the thickness-mode resonance and its value is more difficult to determine (see Sec. IV for more details).
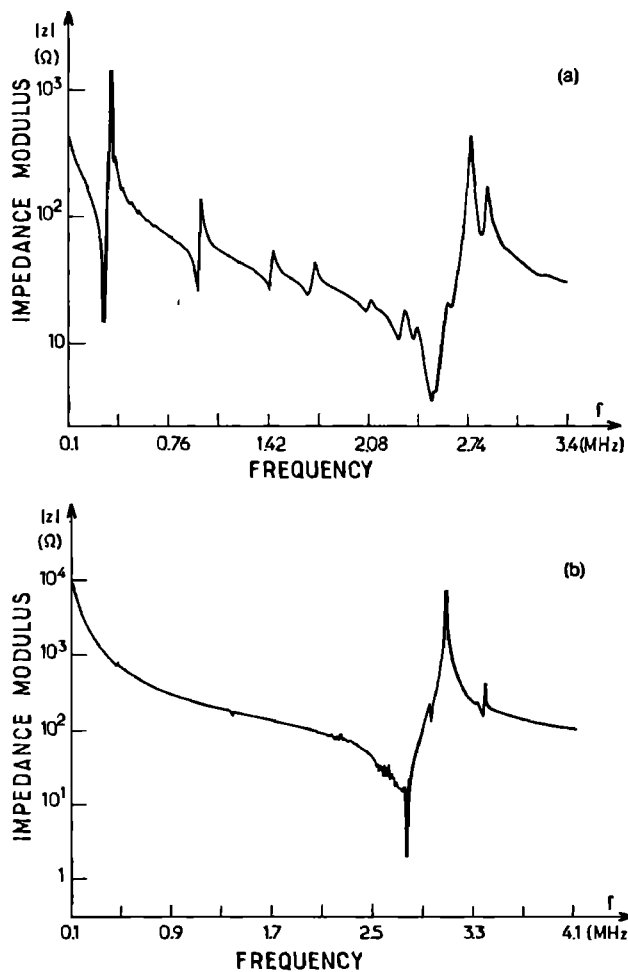


FIG. 6. The measured electrical impedance modulus versus frequency. For PXE-5 material, (a) the minimum impedance value is 3.4 $\Omega$ at 2.49 MHz. For C-24 material, (b) the minimum impedance value is 1.9 $\Omega$ at 2.77 MHz.

FIG. 8. Experimental measurements of PXE-5 transducer front plane displacement for different $Z$ values (in mm): (a) $Z = 10$, (b) $Z = 5$, (c) $Z = 0$, (d) $Z = -5$, and (e) $Z = -10$. The transducer was driven at its fundamental thickness-mode frequency with 1-V peak amplitude excitation voltage.
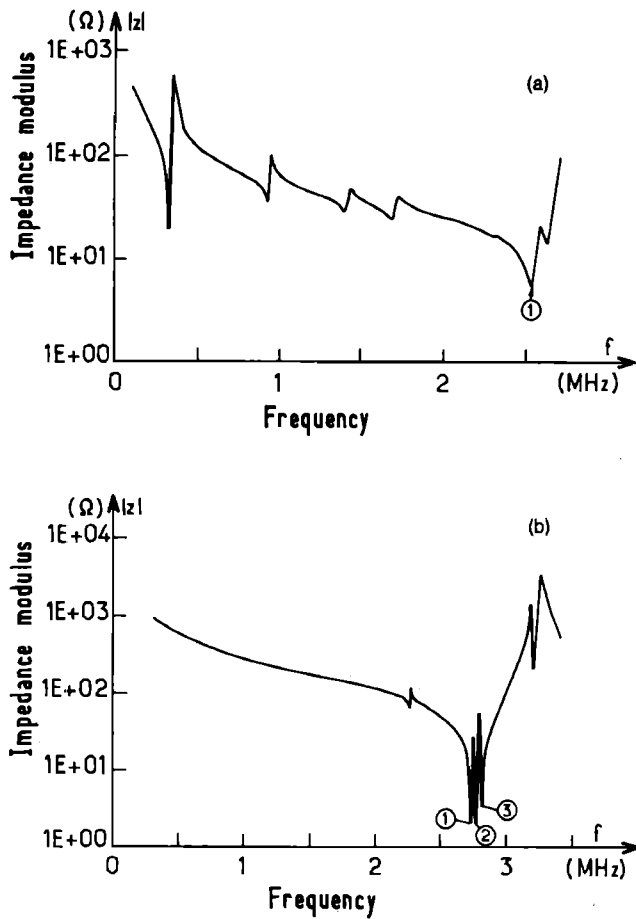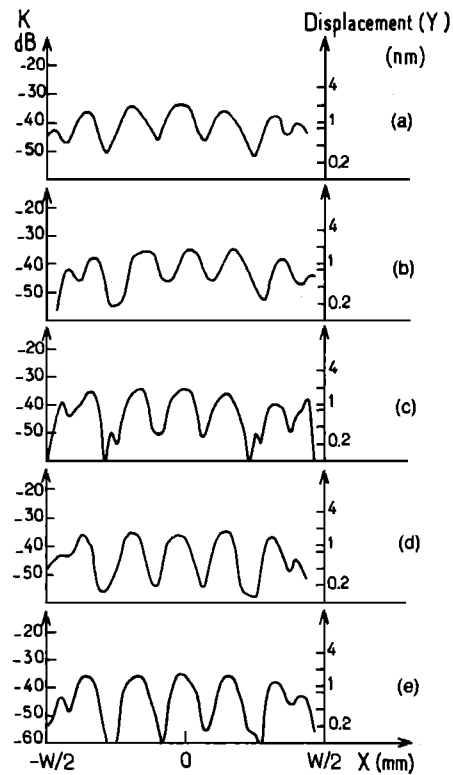
FIG. 7. The simulated electrical impedance modulus versus frequency. The lowest modulus corresponds to the thickness mode. For PXE-5, (a) $|Z| = 5.8\ \Omega$ at 2.522 MHz corresponding to point (1). For C-24, (b) three extremes are obtained: (1) $|Z| = 2\ \Omega$ at 2.736 MHz; (2) $|Z| = 2.2\ \Omega$ at 2.771 MHz; and (3) $|Z| = 3.3\ \Omega$ at 2.817 MHz.

## B. Mechanical displacements
### 1. Optical interferometric measurements

The device holding the transducer is mounted on a micropositioning table having 10-$\mu$m accuracy in each direction. In order to minimize the transducer energy losses, the measurements were made in air. To increase their reflectivities, both transducers were optically polished and their target sides were gold plated by evaporation in a vacuum.

The alignment in each direction was performed by checking the coincidence of the focused laser spot ($\sim 50\ \mu$m in diameter) with the edges of the transducer. The misalignment was found to be less than 1 mrad. Both transducers were driven corresponding to the fundamental thickness-mode piezoelectric resonance of the plate by a 1-V peak amplitude excitation voltage. The transducer translation along the $X$ axis ($\Delta X \sim 100\ \mu$m) allows the measurement of the vibration amplitude $Y(x)$ at a 100-$\mu$m pitch. The experimental results are represented in Figs. 8 and 9.

For PXE-5, the minimum amplitude displacement value obtained at the quarter-width position is 2 nm. The maximum displacement amplitude is 4 nm and is obtained at the middle-width position ($X = 0$). The average displacement amplitude is about 1.75 nm.

In the case of C-24, the minimum displacement value is
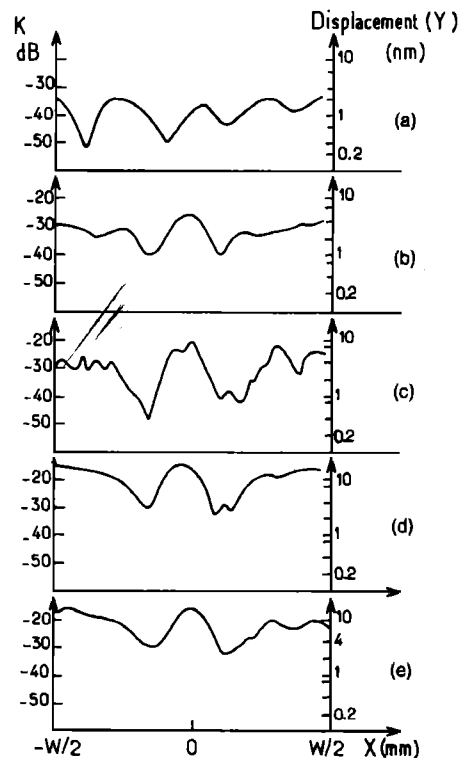


FIG. 9. Same as for Fig. 8, but for C-24. The frequency, corresponding to the minimum electrical impedance, was 2.765 MHz.

Gindre *et al.*: Displacement induced in a piezoelectric structure

| Node | PXE-5 | | C-24 | |
|------|-------|-------|-------|-------|
|      | $X$   | $Y$   | $X$   | $Y$   |
| 53 | 0 | 1.85 | 0 | 19.16 |
| 54 | 1.63 | 2.55 | 10.146 | 14.43 |
| 55 | 2.28 | 3.75 | 14.94 | 3.57 |
| 56 | 1.82 | 3.99 | 12.15 | 6.66 |
| 57 | 0.75 | 3.32 | 3.68 | 9.69 |
| 58 | 0.6 | 3.026 | 5.94 | 5.195 |
| 59 | 2.05 | 3.55 | 12.37 | 3.77 |
| 60 | 3.39 | 3.7 | 13.65 | 9.88 |
| 61 | 3.93 | 2.6 | 10.47 | 12.28 |
| 62 | 3.13 | 1.0 | 4.75 | 12.22 |
| 63 | 1.43 | 0.517 | 1.249 | 12.4 |
| 64 | 0.368 | 1.25 | 5.832 | 13.61 |
| 65 | 1.14 | 2.07 | 7.317 | 14.1 |
| $\langle Y \rangle$ | | 2.56 | | 10 |
| $Y_{max}$ | | 4 | | 19 |
| $Y_{min}$ | | 0.52 | | 9.7 |

## 2. Simulation of mechanical deformation

As stated above, because of the symmetry assumption of symmetry about the median plane of the samples, only a positive quadrant was used in both simulation and graphic representation. Table II gives the values of the nodal displacement modules of electrode nodes apart from their unperturbed position.

For C-24, the average displacement is 10.54 nm, its minimum value is 3.7 nm, and the maximum is found to be $\sim 19$ nm. For PXE-5, these values are 2.56, 0.52, and 4 nm, respectively.

In Figs. 10 and 11, we have represented the maximum displacement of the nodes superposed to the undisturbed node network, for C-24 and PXE-5, respectively.

## IV. DISCUSSION

For PXE-5, we note a good overall correlation obtained between the simulated and experimental curves of the impedance modulus $|Z|$ versus frequency (Figs. 6 and 7). The experimental value of the fundamental thickness-mode frequency $f_0$ is 2.493 MHz and the corresponding measured impedance modulus $|Z|(f_0) = 3.4$ Ω. The simulated curve

0.4 nm and is obtained at the third-width position. The maximum displacement amplitude value is 10 nm and is obtained at the middle-width position. The average displacement amplitude is about 3.79 nm.

The evolution of these displacement profiles along the $L(Z)$ axis has also been investigated. Figure 8 shows this evolution for PXE-5. Note that the displacement profile is nearly constant along the length. For C-24, the profile strongly depends on $L$ (Fig. 9); moreover, we note a loss of symmetry for one of the extremities. The largest displacement magnitude is observed at $L = 21.5$ mm. For this value of $L$, the maximum amplitude (20 nm) is observed in the neighborhood of the middle-width position, a minimum amplitude (3.5 nm) is obtained at a position close to the third of the width, and we derive an average displacement of about 11 nm.
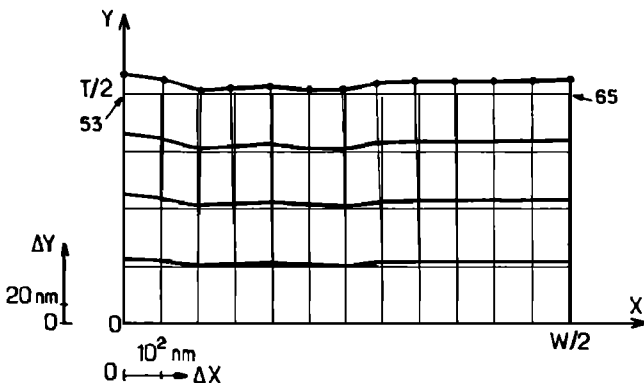
FIG. 10. Simulated mechanical displacement for C-24 superposed to the undisturbed node network, as obtained by the finite element method. The excitation voltage is 1-V peak at 2.817 MHz.
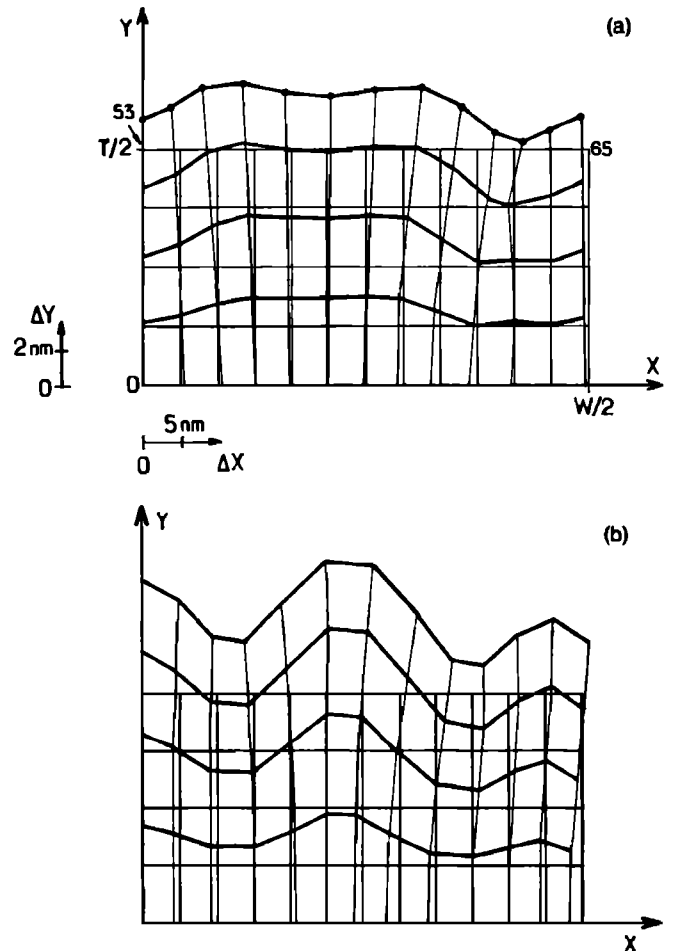
FIG. 11. (a) Same as Fig. 10, but for PXE-5; $f = 2.529$ MHz. (b) Same as (a), but the $C_{13}$ constant is lowered by 20%. The simulated profile is now close to the measured one (cf. Fig. 8).

leads to $f_0 = 2.522$ MHz and to $|Z|(f_0) = 5.8\ \Omega$. The small discrepancy in $f_0$ values is not sensitive to the real thickness of the sample; thus, with $T = 0.822$ instead of 0.800 mm, the simulated value ($f_0 = 2.46$ MHz) is still at about a 3% error compared to the experimental one. The discrepancy between the measured and simulated values of $|Z|(f_0)$ remains significant. This may be due to the weak frequency resolution that has been used in the present simulation and to the value of the loss factor $g$ that has just been estimated.

There is excellent agreement between measured and simulated values of the maximum displacement of the front surface of the PXE-5 transducer. However, the estimated minimum displacement is 2.5 times the measured one. This leads to an overestimation ($\sim 30\%$) of the average amplitude displacement. The most striking discrepancy between the simulation and the experimental data is observed when the shapes of displacement profiles are compared. Whereas the experimental measurements show a maximum displacement in the center of the sample, the simulated curve presents a minimum at the same point. It must be pointed out, however, that a 20% variation in the piezoelectric constant $C_{13}$ value used in the simulation will lead to a simulation profile close to the experimental one [cf. Fig. 11(b)]. Such an inaccuracy can be observed in the determination of ten-
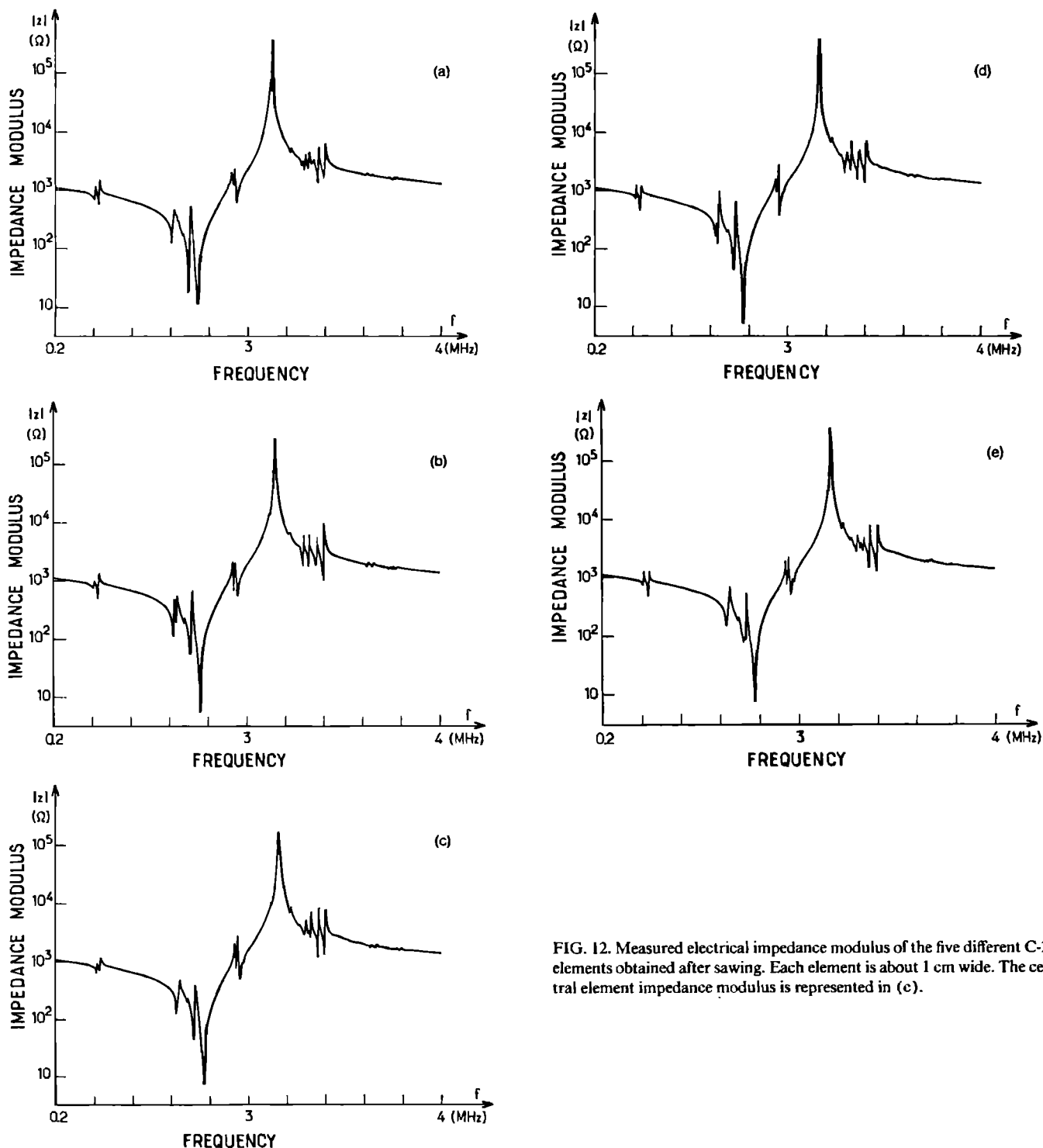


FIG. 12. Measured electrical impedance modulus of the five different C-24 elements obtained after sawing. Each element is about 1 cm wide. The central element impedance modulus is represented in (c).

sorial components of piezoelectric materials. In fact, in these measurements some of the constants like $C_{13}$ are obtained by using a combination of experimental results that are rarely determined with an accuracy better than 5%.

In the case of C-24, the shapes of displacement profiles are similar, but the measured values of displacement ($Y$) strongly depend on the $L$ position. The agreement with simulated values is obtained for $L = 21.5$ mm (i.e., 5 mm from the midposition). The measured values, $Y_{max} = 20$ nm, $Y_{min} = 3.5$ nm, and $\langle Y \rangle \sim 11$ nm, respectively, have to be compared with the simulated ones: $Y_{max} = 19$ nm, $Y_{min} = 3.7$ nm, and $\langle Y \rangle \sim 10.5$ nm. The excellent agreement between the measured and simulated values might be fortunate: Indeed, because of the strong variation of the measured displacement values with $L$ and the observed difference between the simulated and the experimental curves of $|Z|(f)$, we suspect that this transducer was made with a highly inhomogeneous material. In order to check the validity of this hypothesis, we sawed the C-24 sample into five parts and performed impedance modulus measurements on each element.

The results presented in Fig. 12 clearly show, for each individual element, a triplet resonance frequency predicted by simulation. The position of the triplet varies from one sample to another; the triplet lowest impedance modulus moves from 2.735 MHz for sample No. 1 to 2.775 MHz for sample No. 4. This may explain the discrepancy between the measured and simulated values (Figs. 6 and 7). Roughly speaking, the C-24 material may be considered as a sum of individual, slightly different resonant networks, each with a different quality factor $Q$. Thus the equivalent network of the transducer under study presents a "resultant" resonance frequency leading to a simple minimum.

## V. CONCLUSION

From the knowledge of piezoelectric material tensorial parameters, one can predict the behavior of parallelepipedic transducers. The predicted characteristics—impedance versus frequency and the shape of front surface deformation of vibrating transducers—were compared with experimental values.

For both materials studied here, we observe fairly good agreement between the expected and the measured shapes of impedance versus frequency curves, and the fundamental thickness-mode resonance frequency is determined with an accuracy better than 5%. Furthermore, we have shown that any discrepancy between the predicted and the measured shape of the impedance curve strongly indicates the inhomogeneity of the material under study, as was the case for C-24. This inhomogeneity was also detected by interferometric measurements of the vibration displacements of the transducer front plane. Here again, the predicted and measured values of the maxima and minima of the amplitude of vibration are in reasonably fair agreement. The most striking discrepancy comes from the comparison between the simulated and measured deformation profile. The experimental measurements show a maximum displacement in the center of the front plane of the transducer, whereas the simulation

leads to a minimum. However, as we stated above, a variation of 20% in the value of some tensorial parameters used in the simulation gives a more consistent picture of the transducer vibration. Thus extreme care must be taken to avoid any bias in the characteristics used in the simulation. In fact, 1% accuracy in the tensorial components used in the simulation is needed to correctly fit the experimental data. This could be done by increasing the number of one-dimensional samples used in the classical characterization method,[11] and by taking into account the anisotropy of mechanical and electrical losses.[12]

## APPENDIX: RELATION BETWEEN $g$ AND $Q_m$

Here, $Q_m$ is defined as the ratio of the real and imaginary parts of the complex Young's modulus.[13] In the case of a free one-dimensional nonpiezoelectric material, the descriptive equations in the Fourier domain are

$$T(X,\omega) = C^*(j\omega)S(x,\omega) , \tag{A1}$$

$$\frac{\partial T(x,\omega)}{\partial x} = -\omega^2 \rho U(x,\omega) , \tag{A2}$$

$$S(x,\omega) = \frac{\partial U(x,\omega)}{\partial x} . \tag{A3}$$

Equation (A1) is the rheological equation and correspondence to the relation between the stress $T(x,\omega)$ and the strain $S(x,\omega)$, and $C^*(j\omega) = C(1 + j/Q_m)$ is the complex Young's modulus, where $C$ is the elastic coefficient and $Q_m$ the mechanical loss factor as defined previously. Equation (A2) is the mechanical balance, where $\rho$ is the mass density and $U(x,\omega)$ is the Fourier transform of the mechanical displacement. Equation (A3) is the relation between strain and mechanical displacement.

After some elementary substitutions, one gets

$$C^*(j\omega)\frac{\partial^2 U}{\partial x^2} = -\rho\omega^2 U , \tag{A4}$$

which is the one-dimensional wave propagation equation in the Fourier domain.

In terms of the finite element,[6] Eq. (A4) becomes

$$K^*U - \omega^2 MU = 0 , \tag{A5}$$

where $M$ is the mass matrix and $K^*$ is the complex elastic stiffness matrix that can be expressed in the following form:

$$K^* = (1 + 1/jQ_m)K , \tag{A6}$$

where $K$ is the real elastic stiffness matrix. By substitution of (A6) into (A5), we obtain

$$KU + j(1/Q_m)KU - \omega^2 MU = 0 . \tag{A7}$$

If we consider now Eq. (8) expressed for a free ($F = 0$) nonpiezoelectric material ($H_{u\phi} = 0, H_{uu} = K_{uu}$), we derive

$$K_{uu}U + jgK_{uu}U - \omega^2 M_{uu}U = 0 . \tag{A8}$$

Identification between (A7) and (A8) leads to

$$g = 1/Q_m. \tag{A9}$$

On the other hand, in Eq. (A7), the friction force is $(j/Q_m)KU$ and is related to the elastic force $KU$.

In piezoceramics (and contrary to piezoplastics), $Q_m$ is independent of frequency,[14] which implies that the friction force is proportional to and in quadrature with the elastic force.

[1]J. Donjon, "The place of ultrasonics in medical imaging," Acta Electron. **25**, 293 (1983).

[2]C. Mequio, R. H. Coursant, and P. Pesque, "Simulation of the acousto-electric response of piezoelectric structures by means of fast Fourier transform algorithms," Acta Electron. **25**, 311 (1983).

[3]J. F. Gelly, A. Gardin, and C. Maerfeld, "A two dimensional model for the acoustical field generated by linear array used in $B$-scan echography," in *Proceedings of the IEEE Ultrasonic Symposium*, 27–29 October 1982, San Diego, CA (IEEE, New York, 1982), p. 805.

[4]R.H. Coursant, J. M. Tellier, and M. Naillon, "Characterization of piezoelectric ceramics used in multielement ultrasonic transducers for medical imaging," in *Proceedings of Ultrasonic International 85*, 2–4 July 1985, London (Butterworth, Guildford, U. K., 1985), p. 563.

[5]R. L. Jungerman, P. Benett, A. R. Selfridge, B. T. Khuri-Yakub, and G. S. Kino, "Measurement of normal surface displacement for the characterization of rectangular acoustic array elements," J. Acoust. Soc. Am. **76**, 516 (1984).

[6]The name of the software package is PERMAS. It was derived from ASKA software and extended to piezoelectric deformation calcula-tion by L. E. P. in collaboration with C. I. S. I. (35 Bd. Brune, 75680 Paris Cedex 14, France); cf. M. Naillon, R. H. Coursant, and F. Besnier, "Analysis of piezoelectric structures by a finite element method," Acta Electron. **25**(4), 341 (1983).

[7]For a review article, see J. P. Montchalin, "Optical detection of ultrasound," in IEEE Trans. Ultrason. Ferroelectr. Freq. Control UFFC **33**(5), 485 (1986).

[8]See, for example, D. Boucher, M. Lagier, and C. Maerfeld, "Computation of the vibrational modes for piezoelectric array transducers using a mixed finite element–perturbation method," IEEE Trans. Sonics Ultrason. SU-**28**(5), 318 (1981); O. C. Zienkiewicz, *The Finite Element Method* (McGraw-Hill, New York, 1977).

[9]P. G. Ciarlet, *The Finite Element Method for Elliptic Problems* (North-Holland, Amsterdam, The Netherlands, 1979).

[10]P. G. Ciarlet, *Introduction á l'analyse numérique matricielle et á l'optimisation* (Masson et Cie Editeurs, Paris, 1982).

[11]R. Holland and E. P. Eer Nisse, "Accurate measurement of coefficients in ferroelectric ceramic," IEEE Trans. Sonics Ultrason. SU-16(4), 173 (1969).

[12]R. H. Coursant, P. Eyraud, L. Eyraud, M. Fink, and J. M. Tellier, "Preparation and characterization of lead titanate and lead metaniobate piezoceramic for ultrasonic tranducer design," in *Proceedings of the 6th IEEE International Symposium on the Application of Ferroelectrics*, 9–11 June 1986, Lehigh University (IEEE, New York, 1986), p. 442.

[13]H. J. McSkimin, "Ultrasonic method for measuring the mechanical properties of liquids and solids," in *Physical Acoustics*, edited by W. P. Mason (Academic, New York, 1964), Vol. I, part A, Chap. 4, p. 274.

[14]R. H. Coursant, "Simulation of the acousto-electric response of ultrasonic narrow strip transducers with mechanical losses," in *Proceedings of Ultrasonics International 83*, 12–14 July 1980, Halifax, Canada (Butterworth, Guildford, U. K., 1980), pp. 414–419.